THE ASTRONOMICAL JOURNAL, 115:2337–2344, 1998 June

SPECTROSCOPY OF GLOBULAR CLUSTERS IN NGC 4472

R. M. SHARPLES
Department of Physics, University of Durham, South Road, Durham DH1 3LE, England, UK

S. E. ZEPF[1]
Department of Astronomy, University of California at Berkeley, Berkeley, CA 94720; and Department of Astronomy, P.O. Box 208101, Yale University, New Haven, CT 06520

T. J. BRIDGES
Royal Greenwich Observatory, Madingley Road, Cambridge CB3 0EZ, England, UK

D. A. HANES[2]
Department of Physics, Queen's University, Kingston, ON K7L 3N6, Canada

D. CARTER
Astrophysics Research Institute, School of Engineering, Liverpool John Moores University, Byrom Street, Liverpool L3 3AF, England, UK

K. M. ASHMAN
Department of Physics and Astronomy, University of Kansas, Lawrence, KS 66045

AND

D. GEISLER
Kitt Peak National Observatory, National Optical Astronomy Observatories, 950 North Cherry Avenue, Tucson, AZ 85726
Received 1997 December 23

ABSTRACT

Optical multislit spectra have been obtained for 47 globular clusters surrounding the brightest Virgo elliptical galaxy, NGC 4472 (M49). Including data from the literature, we analyze velocities for a total sample of 57 clusters and present the first tentative evidence for kinematic differences between the red and blue cluster populations that make up the bimodal color distribution of this galaxy. The redder clusters are more centrally concentrated and have a velocity dispersion of 240 km s^{-1}, compared with 320 km s^{-1} for the blue clusters. The origin of this difference appears to be a larger component of systematic rotation in the blue cluster system. The larger rotation in the more extended blue cluster system is indicative of efficient angular momentum transport, as provided by galaxy mergers. Masses estimated from the globular cluster velocities are consistent with the mass distribution estimated from X-ray data and indicate that the M/L_B rises to 50 $(M/L)_\odot$ at $2.5R_e$.

Key words: galaxies: fundamental parameters — galaxies: kinematics and dynamics — galaxies: star clusters — globular clusters: individual (NGC 4472)

1. INTRODUCTION

The study of extragalactic globular cluster systems can provide important clues to the formation history of their host galaxies. This is particularly true for elliptical galaxies, for which there are two currently popular paradigms. One paradigm is the standard monolithic-collapse model, in which elliptical galaxies form in a single burst of star formation at high redshift (e.g., Arimoto & Yohii 1987). In contrast, hierarchical structure formation theories predict that spheroidal galaxies form continuously through a sequence of galaxy mergers (e.g., Cole et al. 1994; Kauffmann 1996). Ashman & Zepf (1992, 1997) explored the properties of globular clusters in models in which elliptical galaxies are the products of the mergers of spiral galaxies and showed that the greater specific frequency of globular clusters around elliptical galaxies relative to spiral galaxies could be explained if globular clusters form during the mergers. They also predicted that elliptical galaxies formed by mergers will have two or more populations of globular clusters—a metal-poor population associated with the progenitor spiral galaxies and a metal-rich population formed during the merger. In contrast, monolithic-collapse models naturally produce unimodal metallicity distributions. The discovery that the globular cluster systems of several elliptical galaxies have bimodal color (and, by implication, metallicity) distributions (Zepf & Ashman 1993; Whitmore et al. 1995; Geisler, Lee, & Kim 1996) provides strong support for the merger model. Geisler et al. (1996) and Lee, Kim, & Geisler (1998) also show that the red (metal-rich) cluster population is more centrally concentrated than the blue (metal-poor) population, as predicted by Ashman & Zepf (1992).

Recently, an alternative view has been presented by Forbes, Brodie, & Grillmair (1997), who suggest that the bimodal color distributions may be due not to mergers but to a multiphase collapse. Although the primary physical mechanism known to produce distinct formation episodes is mergers, it is important to attempt to distinguish between these competing models for the formation of globular cluster systems and their host elliptical galaxies. The kinematics of globular cluster systems may offer such a test of these models. In the multiphase collapse picture, conservation of angular momentum requires that the spatially concentrated metal-rich population rotate more rapidly than the extended metal-poor population. In contrast, simulations of merger models indicate that mergers typically provide an efficient means of angular momentum transfer,

[1] Hubble Fellow.
[2] Visiting Astronomer, William Herschel Telescope. The WHT is operated on the island of La Palma by the Isaac Newton Group in the Spanish Observatorio del Roque de los Muchachos of the Instituto de Astrofísica de Canarias.

and that the central regions have specific angular momentum that is lower than the outer regions (Hernquist 1993; Heyl, Hernquist, & Spergel 1996).

Studies of the kinematics of globular cluster systems therefore provide important constraints on the formation history of elliptical galaxies. They also provide useful probes of the mass distribution of elliptical galaxies at radii larger than can be reached by studies of the integrated light. The extended nature of globular cluster systems allows the dynamical mass determined from their velocities to be compared at similar radii with masses determined through studies of the hot X-ray gas. A recent example is the study of the M87 globular cluster system by Cohen & Ryzhov (1997), who find that a rising mass-to-light ratio is required out to radii of $\sim 3R_e$, in agreement with X-ray mass determinations. However, M87 occupies a privileged position at the center of the Virgo Cluster, so it is critical to test whether the rising mass-to-light ratio, and the agreement with X-ray masses, is true for more typical cluster elliptical galaxies.

In this paper, we present a spectroscopic study of the globular cluster system of the elliptical galaxy NGC 4472 (M49). This is the brightest elliptical galaxy in the Virgo Cluster and has been the subject of a detailed photometric study by Geisler et al. (1996). The only previously published spectroscopic data for the NGC 4472 globular cluster population is by Mould et al. (1990), who presented velocities and line strengths for 26 clusters.

The outline of our paper is as follows: Section 2 discusses the sample selection together with our observations and data reduction; § 3 discusses the kinematics of the metal-rich and metal-poor populations in the context of the merger model and analyzes the implications for the overall mass-to-light ratio in NGC 4472. Finally, we present our conclusions in § 4.

2. OBSERVATIONS AND DATA REDUCTION

Geisler et al. (1996) have made a deep ($R \sim 25$) photometric study of the globular cluster system surrounding NGC 4472 in the integrated Washington CT_1 system. They showed that the color distribution was clearly bimodal and could be fitted well by two Gaussians with peaks at $C - T_1 = 1.32$ and 1.81, corresponding to metallicities of [Fe/H] $= -1.3$ and -0.1. We selected our sample for spectroscopic study from a preliminary version of the Geisler et al. (1996) catalog. In order to avoid any biases in the spectroscopic cluster sample, particularly with regard to the presence of any young cluster population, we have applied only a very broad color cut of $0.5 < C - T_1 < 2.2$, together with a magnitude cut of $19.5 \leq V \leq 22.5$ to the original catalog, where $V \simeq T_1 + 0.5$ (Geisler 1996). The color distribution of this sample is shown in Figure 1. Because the catalogs are incomplete near the bright central parts of the galaxy, the multislit masks were offset along the major axis of the galaxy by $\sim 3'$ in order to maximize the spatial and spectral coverage of the samples.

Spectroscopic observations of 79 cluster candidates were obtained with the Low-Dispersion Survey Spectrograph (LDSS-2; Allington-Smith et al. 1994) on the 4.2 m William Herschel Telescope in 1994 April. Further details of the observing setup are given in Table 1 and in Bridges et al. (1997). Dome and twilight flats were taken at the beginning and end of each night, and the spectra were wavelength-calibrated using frequent CuAr arcs. Long slit spectra of the Galactic globular clusters M92 (NGC 6341; [Fe/H] $= -2.24$), M13 (NGC 6205; [Fe/H] $= -1.65$), NGC 6356 ([Fe/H] $= -0.54$), and the radial velocity standards HD 194071 (G8 III) and HD 132737 (K0 III) were taken for velocity and metallicity calibration. Data reduction for the first mask followed closely the procedures detailed in Bridges et al. (1997) using the LEXT (Allington-Smith et al. 1994) software package. A third-order polynomial fit to the arc spectra yielded residuals of ~ 0.13 Å (8 km s^{-1}), and the spectra were rebinned to linear and logarithmic wavelength scales over the wavelength range 3800–6000 Å with a bin size of 2.0 Å. The spectra were then optimally extracted and sky-subtracted, using linear fits for the background sky.

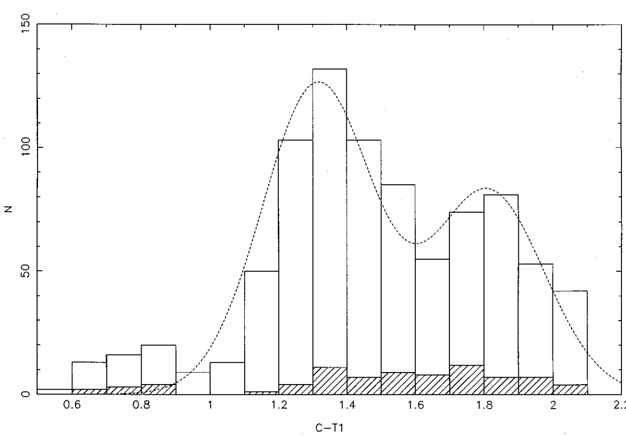

FIG. 1.—Color distribution for globular cluster candidates with $19.5 < V < 22.5$ and $0.5 < C - T_1 < 2.2$ from Geisler et al. (1996). The open histogram is for the full sample of 860 candidates from which our spectroscopic targets were selected; the hatched histogram is for the 79 objects for which spectra were obtained.

For the other two masks a slightly different procedure was followed. Rather than adjust the individual multislit lengths to fill the available mask dimensions, a fixed-length multislit of 8″ was adopted, and the targets were nodded up and down the slits by $\pm 2''.5$ on consecutive exposures. This procedure allowed us to substantially increase the number of objects observed per mask and, by differencing pairs of exposures to subtract the sky background, removed some of the systematic effects due to flat-fielding and irregularities in the slit profiles during this crucial stage. Comparison of spectra for objects observed on more than one mask (§ 2.1) indicated that this technique does not degrade the signal-to-noise ratio (S/N) achieved and substantially increased the efficiency of our observations.

2.1. *Radial Velocities and Confirmed Globular Clusters*

Radial velocities were obtained by cross-correlating with the template spectra of M13, M92, NGC 6356, HD 132737,

TABLE 1

LOG OF OBSERVATIONS

Parameter	Value
Dates	1994 April 11–14
Telescope/instrument	4.2 m WHT/LDSS-2
Dispersion (resolution)	2.4 Å pixel^{-1} (6 Å FWHM)
Detector	1024^2 TEK CCD
Wavelength coverage (max)	3800–6000 Å
Seeing	1″–2″
Exposure time (mask 1/2/3)	3.0/3.5/3.5 hr
Number of objects (mask 1/2/3)	21/38/38

and HD 194071 and forming a weighted average of the results after rejecting poor matches (normalized correlation amplitudes less than 0.15). Velocities for the template clusters were taken from Hesser, Shawl, & Meyer (1986). Cross-correlation of spectra from the twilight sky frames indicated an rms velocity uncertainty of 37 km s^{-1} for high-S/N data; this was added in quadrature to the scatter between templates to give the final velocity errors in Table 2. Eleven objects were measured on more than one mask and have an rms velocity difference of 54 km s^{-1}, which is consistent with the estimated velocity errors. Table 2 contains positions, color, and magnitudes for 79 cluster candidates for which spectra were obtained, together with velocities and velocity errors for 55 objects with reliable cross-correlation results (generally against three or more templates). The astrometric solution was obtained from a fit to 43 secondary standards distributed across the field, and the relative positions should be good to $\pm 0\farcs3$. The color distribution of the 55 objects with radial velocities is shown in Figure 2.

A histogram of the radial velocities of these 55 objects is given in Figure 3. Following Mould et al. (1990) we take the velocity range 300 km s^{-1} < $V_{\rm hel}$ < 2000 km s^{-1} as

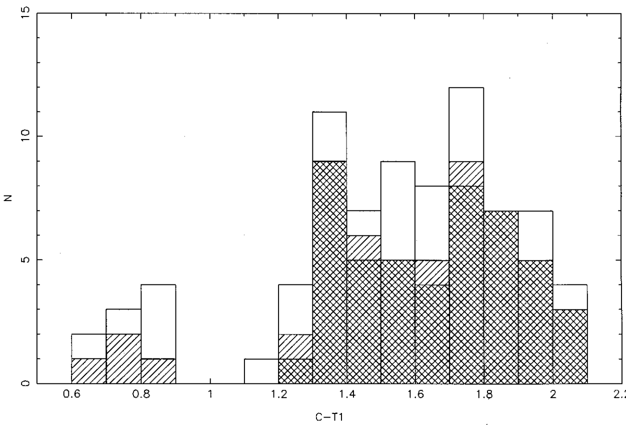

FIG. 2.—The open histogram shows the color distribution for the 79 globular cluster candidates for which spectra were obtained. The hatched histogram shows the 55 candidates for which reliable velocities were derived from the cross-correlation analysis. The cross-hatched area shows the color distribution of the 47 objects identified as clusters on the basis of their radial velocities in Table 2.

TABLE 2

VELOCITIES OF GLOBULAR CLUSTER CANDIDATES IN NGC 4472

ID	T_1	$C-T_1$	$V_{\rm hel}$ (km s^{-1})	R.A. (B1950.0)	Decl. (B1950.0)	ID	T_1	$C-T_1$	$V_{\rm hel}$ (km s^{-1})	R.A. (B1950.0)	Decl. (B1950.0)
1407......	21.89	1.28	-8 ± 44	12 27 04.91	8 12 46.4	5263......	19.91	0.77	-88 ± 40	12 27 03.22	8 17 30.0
1483......	20.75	1.56	...	12 27 12.94	8 12 57.8	5323......	20.33	0.82	...	12 27 16.29	8 17 33.8
1518......	19.25	1.85	1050 ± 36	12 27 07.89	8 13 00.5	5511......	21.17	1.74	...	12 27 17.31	8 17 44.7
1650......	20.85	1.95	...	12 27 23.29	8 13 13.4	5561......	20.82	1.39	903 ± 48	12 26 56.84	8 17 48.3
1712......	20.36	1.34	1144 ± 40	12 27 07.54	8 13 18.9	5629......	21.09	1.36	522 ± 52	12 27 11.90	8 17 52.2
2031......	20.71	1.37	...	12 27 15.12	8 13 46.3	5673......	21.73	1.25	...	12 27 20.81	8 17 54.2
2045......	20.94	1.77	857 ± 54	12 27 06.50	8 13 47.7	5943......	21.07	1.56	...	12 27 11.46	8 18 11.6
2140......	20.45	1.80	730 ± 53	12 27 21.64	8 13 55.3	6164......	19.79	1.65	426 ± 30	12 27 12.25	8 18 27.1
2163......	20.15	2.01	402 ± 43	12 27 23.34	8 13 57.6	6284......	19.44	1.57	569 ± 54	12 27 25.39	8 18 36.8
2178......	21.51	1.19	...	12 27 04.82	8 13 59.0	6294......	21.02	1.64	1034 ± 84	12 27 01.30	8 18 37.7
2306......	20.35	1.62	...	12 27 25.13	8 14 09.0	6427......	21.11	1.79	1141 ± 50	12 27 12.47	8 18 47.5
2341......	20.76	1.91	1001 ± 68	12 27 00.21	8 14 12.9	6520......	20.06	1.86	607 ± 57	12 27 16.75	8 18 53.5
2406......	20.84	2.03	1244 ± 70	12 27 13.23	8 14 18.4	6564......	20.03	1.34	1077 ± 31	12 27 10.77	8 18 57.2
2482......	21.58	2.08	767 ± 56	12 27 10.16	8 14 24.6	6696......	20.08	1.59	550 ± 52	12 27 21.45	8 19 08.5
2543......	20.27	1.36	1199 ± 48	12 27 20.33	8 14 29.3	6721......	21.09	1.73	1180 ± 45	12 27 07.36	8 19 10.5
2569......	20.12	1.89	1056 ± 46	12 27 11.32	8 14 31.7	6872......	20.15	1.46	870 ± 41	12 27 09.21	8 19 20.7
2634......	19.70	1.56	1014 ± 57	12 27 07.08	8 14 37.9	6989......	20.61	1.75	1071 ± 50	12 27 21.98	8 19 30.5
2679......	21.38	1.59	...	12 27 19.00	8 14 41.5	7174......	21.01	1.51	...	12 27 20.43	8 19 46.3
2757......	19.62	1.45	-79 ± 37	12 27 08.35	8 14 47.2	7197......	20.94	1.50	782 ± 50	12 27 08.44	8 19 48.2
2860......	20.27	1.21	...	12 27 22.00	8 14 52.5	7340......	20.91	1.77	1308 ± 124	12 27 17.39	8 19 59.0
3119......	20.78	1.74	11068 ± 50	12 27 15.44	8 15 09.9	7399......	20.35	1.40	1005 ± 44	12 27 01.33	8 20 05.1
3150......	21.40	1.79	952 ± 42	12 27 05.95	8 15 12.1	7458......	20.75	1.84	807 ± 57	12 27 12.23	8 20 08.6
3323......	21.29	1.60	12321 ± 50	12 27 26.82	8 15 22.8	7615......	21.13	1.68	...	12 27 11.53	8 20 20.2
3412......	19.83	0.72	-203 ± 38	12 27 09.07	8 15 30.1	7659......	19.87	1.34	1571 ± 56	12 27 10.54	8 20 24.0
3592......	20.15	0.79	...	12 27 16.91	8 15 41.4	7731......	19.55	0.82	151 ± 48	12 27 19.33	8 20 30.2
3628......	21.22	1.90	1008 ± 49	12 27 00.59	8 15 43.9	7784......	19.20	1.52	868 ± 51	12 27 23.22	8 20 34.4
3789......	19.52	1.70	...	12 27 30.22	8 15 53.6	7894......	21.61	1.73	730 ± 81	12 27 01.99	8 20 37.2
3808......	20.35	1.83	832 ± 35	12 27 06.60	8 15 54.5	7938......	20.92	1.44	1251 ± 50	12 27 11.90	8 20 47.7
3865......	21.60	0.80	...	12 27 02.92	8 16 17.2	8090......	20.51	1.46	903 ± 66	12 27 13.14	8 21 00.9
3980......	21.15	1.28	1112 ± 45	12 27 03.05	8 16 05.4	8165......	20.22	1.39	1027 ± 47	12 27 23.57	8 21 06.8
4017......	20.92	1.42	...	12 27 25.05	8 16 07.8	8228......	21.48	1.77	...	12 27 09.19	8 21 11.9
4168......	20.36	1.68	1384 ± 44	12 27 07.64	8 16 19.4	8353......	20.03	1.98	928 ± 40	12 27 08.71	8 21 22.8
4386......	19.83	1.94	1197 ± 33	12 27 19.16	8 16 34.7	8384......	21.39	1.41	768 ± 54	12 27 15.30	8 21 24.4
4513......	20.10	1.85	908 ± 80	12 27 09.77	8 16 42.7	8516......	21.82	2.01	...	12 27 05.28	8 21 36.6
4542......	20.62	0.68	...	12 27 22.64	8 16 44.5	8665......	19.60	0.69	-218 ± 35	12 27 11.86	8 21 50.6
4731......	19.96	1.43	698 ± 57	12 27 09.55	8 16 58.1	8890......	20.41	1.88	870 ± 65	12 27 15.77	8 22 14.0
4780......	19.52	1.95	971 ± 45	12 27 20.79	8 17 00.9	8909......	21.91	1.40	...	12 27 02.41	8 22 15.3
4959......	21.38	1.33	1449 ± 44	12 27 23.05	8 17 11.9	9009......	21.28	1.99	...	12 27 12.26	8 22 24.1
5090......	19.83	1.61	582 ± 46	12 27 09.43	8 17 20.2	9228......	21.01	1.61	...	12 27 09.08	8 22 50.5
5112......	20.35	0.89	...	12 27 16.37	8 17 21.4						

NOTE.—Successive columns give the ID, T_1 magnitude, $C - T_1$ color (from Geisler et al. 1996), heliocentric velocity, velocity error, R.A. (B1950.0), and decl. (B1950.0). Units of right ascension are hours, minutes, and seconds, and units of declination are degrees, arcminutes, and arcseconds.

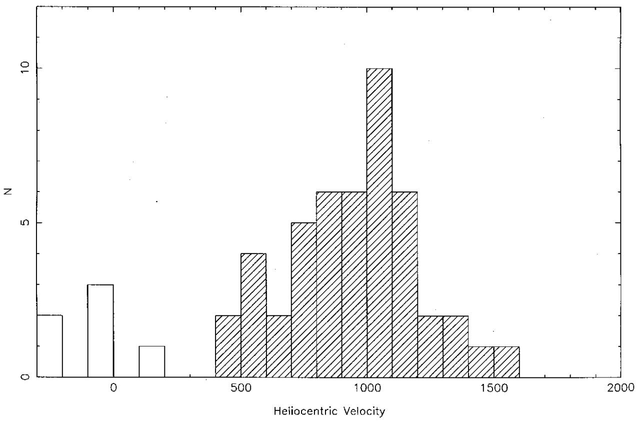

FIG. 3.—Heliocentric velocities for 53 globular cluster candidates around NGC 4472. Two objects (presumably, compact galaxies) with velocities greater than 10,000 km s^{-1} have been omitted. The hatched histogram shows those candidates assumed to be bona fide clusters belonging to NGC 4472 (see text for details).

representative of globular clusters belonging to NGC 4472, which has a recession velocity of 961 km s^{-1} (Sandage & Tammann 1981); the 47 objects in this range have a mean velocity of 943 $\pm$ 38 km s^{-1} and a velocity dispersion of 258 km s^{-1}. Assuming $\sigma = 110$ km s^{-1} for halo subdwarfs (Mould et al. 1990), the lowest velocity object in our cluster sample (2163) has a 4% chance of belonging to the NGC 4472 system and only 0.02% of being a Galactic star; the highest velocity object excluded (7731) has a 17% chance of being a Galactic star and only a 0.2% chance of belonging to the NGC 4472 system. Including or excluding these objects from the cluster sample yields a velocity dispersion in the range 248–279 km s^{-1}.

3. RESULTS

The only previous spectroscopic study of the NGC 4472 globular cluster system is that of Mould et al. (1990), who obtained spectra for 54 candidates from which they identified 26 clusters. The contamination by foreground stars and background stars in their study (49%) is higher than that obtained here (15%), presumably the result of the magnitude and color range adopted. Thirteen objects in Table 2 are in common with the Mould et al. (1990) sample; for 12 of these the radial velocity measurements are in good agreement, with a mean difference of -2 km s^{-1} and a dispersion of 79 km s^{-1}. The remaining object (5090) has a velocity of 582 km s^{-1} as listed in Table 2 and 959 km s^{-1} in Mould et al. (1990); although we only have one spectrum of this object, there are good cross-correlations with all of the templates, and it seems likely that the source of the discrepancy is a misidentification.

Table 3 contains data for the combined sample of 57 clusters. The mean velocity error for the overlap sample from our measurements is 46 km s^{-1}, so we have adopted a typical 1 σ error of $(79^2 - 46^2)^{1/2} = 65$ km s^{-1} for those clusters with velocities from Mould et al. (1990). Where clusters have velocities available from our LDSS-2 data, we list these preferentially because of their smaller formal errors; however, the results presented below do not change significantly if instead the two data sets are averaged. Also indicated in this table is the angular distance of each cluster from the center of NGC 4472 (taken as R.A. = $12^h27^m15^s.0$, decl. = $+08°16'45''$, B1950.0) and the projected distance along the major axis of the elliptical isophotes of the galaxy (taken as P.A. = 162°; Sandage & Tamman 1981). The [Fe/H] values are taken from Geisler et al. (1996).

3.1. *Kinematic Properties*

One of the most important characteristics of the NGC 4472 globular cluster system is the clearly bimodal nature of its color (metallicity) distribution. Geisler et al. (1996) have already demonstrated structural differences between the metal-rich and metal-poor populations, with the metal-rich clusters being significantly more concentrated to the center of NGC 4472 than are their metal-poor counterparts. The primary goal of our study was therefore to search for any kinematic differences between the metal-rich and metal-poor globular cluster populations.

In order to divide the sample, we have run a KMM mixture-modeling test (Ashman et al. 1994), which indicates that the most probable boundary between the metal-rich and metal-poor clusters is at $C - T_1 = 1.625$ or [Fe/H] = -0.57 (cf. Fig. 1). Figure 4 shows the velocity histograms for the 57 clusters in Table 3 divided in this way. The two distributions do indeed appear to be different, with the metal-rich clusters having a lower velocity dispersion; an F-test rejects the hypothesis that the two populations have the same dispersion at the 86% confidence level. Although only tentative given the current sample size, this is a potentially powerful result and would represent the first detection of a velocity dispersion difference in a bimodal globular

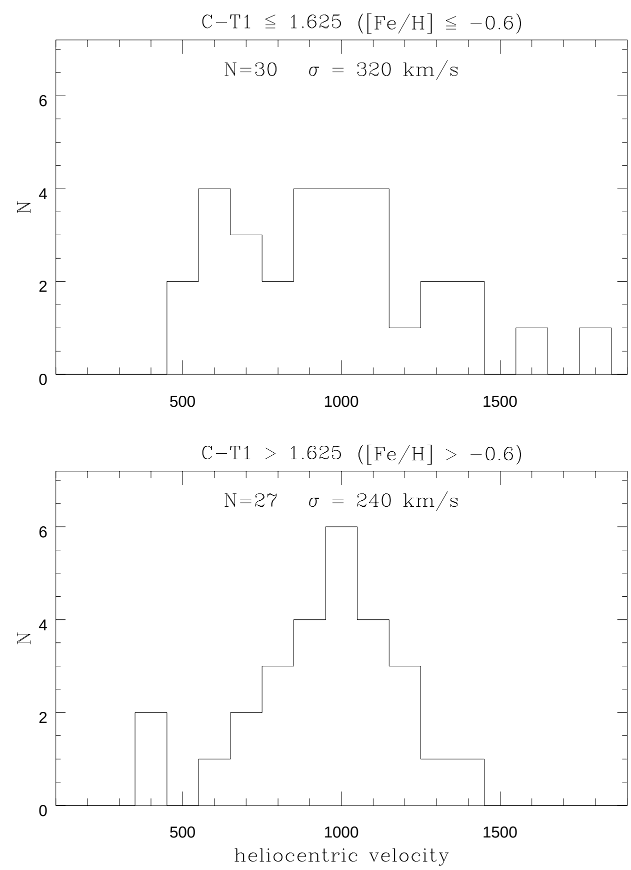

FIG. 4.—Comparison of the velocity distributions of the metal-poor and metal-rich cluster populations in NGC 4472. An F-test rejects the hypothesis that these two have the same dispersion at the 86% confidence level. The mean velocities of the two populations, 969 $\pm$ 58 km s^{-1} (N = 30) and 946 $\pm$ 46 km s^{-1} (N = 27), are identical within the errors.

TABLE 3

CONFIRMED GLOBULAR CLUSTERS IN NGC 4472

ID	T_1	$C - T_1$	V_{hel}	Err	r(arcsec)	r_{maj}(arcsec)	[Fe/H]	R.A. (B1950.0)	Decl. (B1950.0)	Other ID
1518......	19.25	1.85	1050	36	248	181	0.0	12 27 07.89	8 13 00.5	234
1712......	20.36	1.34	1144	40	234	162	−1.2	12 27 07.54	8 13 18.9	
2031......	20.71	1.37	1352[a]	65	178	170	−1.2	12 27 15.12	8 13 46.3	142
2045......	20.94	1.77	857	54	217	129	−0.2	12 27 06.50	8 13 47.7	
2060......	20.62	1.29	1108[a]	65	212	132	−1.3	12 27 07.15	8 13 48.3	243
2140......	20.45	1.80	730	53	196	192	−0.2	12 27 21.64	8 13 55.3	
2163......	20.15	2.01	402	43	208	197	0.3	12 27 23.34	8 13 57.6	
2341......	20.76	1.91	1001	68	267	77	0.1	12 27 00.21	8 14 12.9	
2406......	20.84	2.03	1244	70	149	131	0.4	12 27 13.23	8 14 18.4	
2482......	21.58	2.08	767	56	157	111	0.5	12 27 10.16	8 14 24.6	
2528......	20.34	1.46	654[a]	65	139	138	−1.0	12 27 16.79	8 14 28.2	118
2543......	20.27	1.36	1199	48	157	153	−1.2	12 27 20.33	8 14 29.3	90
2569......	20.12	1.89	1056	46	144	110	0.1	12 27 11.32	8 14 31.7	196
2634......	19.70	1.56	1014	57	173	84	−0.7	12 27 07.08	8 14 37.9	245
3150......	21.40	1.79	952	42	163	46	−0.2	12 27 05.95	8 15 12.1	
3307......	20.25	1.53	1790[a]	65	237	148	−0.8	12 27 29.92	8 15 21.3	19
3628......	21.22	1.90	1008	49	222	−8	0.1	12 27 00.59	8 15 43.9	
3808......	20.35	1.83	832	35	134	9	−0.1	12 27 06.60	8 15 54.5	
3980......	21.15	1.28	1112	45	182	−17	−1.4	12 27 03.05	8 16 05.4	
4168......	20.36	1.68	1384	44	112	−10	−0.4	12 27 07.64	8 16 19.4	
4386......	19.83	1.94	1197	33	63	29	0.2	12 27 19.16	8 16 34.7	
4513......	20.10	1.85	908	80	78	−22	0.0	12 27 09.77	8 16 42.7	
4731......	19.96	1.43	698	57	82	−38	−1.0	12 27 09.55	8 16 58.1	215
4780......	19.52	1.95	971	45	88	11	0.2	12 27 20.79	8 17 00.9	86
4959......	21.38	1.33	1449	44	123	11	−1.3	12 27 23.05	8 17 11.9	
5090......	19.83	1.61	582	46	90	−59	−0.6	12 27 09.43	8 17 20.2	218
5323......	20.33	0.82	1263[a]	65	53	−41	−2.5	12 27 16.29	8 17 33.8	130
5456......	19.26	1.39	737[a]	65	68	−66	−1.1	12 27 12.49	8 17 41.4	177
5561......	20.82	1.39	903	48	277	−144	−1.1	12 26 56.84	8 17 48.3	
5629......	21.09	1.36	522	52	82	−79	−1.2	12 27 11.90	8 17 52.2	
6164......	19.79	1.65	426	30	110	−110	−0.5	12 27 12.25	8 18 27.1	181
6231......	20.77	1.81	1069[a]	65	110	−95	−0.1	12 27 16.54	8 18 32.3	127
6284......	19.44	1.57	569	54	191	−59	−0.7	12 27 25.39	8 18 36.8	40
6294......	21.02	1.64	1034	84	233	−170	−0.5	12 27 01.30	8 18 37.7	
6427......	21.11	1.79	1141	50	128	−128	−0.2	12 27 12.47	8 18 47.5	
6520......	20.06	1.86	607	57	131	−114	0.0	12 27 16.75	8 18 53.5	121
6564......	20.03	1.34	1077	31	147	−146	−1.2	12 27 10.77	8 18 57.2	206
6696......	20.08	1.59	550	52	173	−107	−0.6	12 27 21.45	8 19 08.5	82
6721......	21.09	1.73	1180	45	185	−174	−0.3	12 27 07.36	8 19 10.5	
6872......	20.15	1.46	870	41	178	−175	−1.0	12 27 09.21	8 19 20.7	221
6989......	20.61	1.75	1071	50	196	−126	−0.3	12 27 21.98	8 19 30.5	
7197......	20.94	1.50	782	50	208	−205	−0.9	12 27 08.44	8 19 48.2	
7340......	20.91	1.77	1308	124	197	−173	−0.2	12 27 17.39	8 19 59.0	
7399......	20.35	1.40	1005	44	285	−253	−1.1	12 27 01.33	8 20 05.1	
7458......	20.75	1.84	807	57	208	−207	−0.1	12 27 12.23	8 20 08.6	
7659......	19.87	1.34	1571	56	229	−229	−1.2	12 27 10.54	8 20 24.0	
7784......	19.20	1.52	868	51	260	−181	−0.8	12 27 23.22	8 20 34.4	
7889......	18.84	1.58	614[a]	65	285	−179	−0.7	12 27 25.49	8 20 43.5	I-20
7894......	21.61	1.73	730	81	302	−281	−0.3	12 27 01.99	8 20 37.2	
7938......	20.92	1.44	1251	50	247	−245	−1.0	12 27 11.90	8 20 47.7	
8090......	20.51	1.46	903	66	258	−252	−0.9	12 27 13.14	8 21 00.9	
8165......	20.22	1.39	1027	47	291	−210	−1.1	12 27 23.57	8 21 06.8	
8353......	20.03	1.98	928	40	293	−293	0.3	12 27 08.71	8 21 22.8	
8384......	21.39	1.41	768	54	280	−265	−1.1	12 27 15.30	8 21 24.4	
8890......	20.41	1.88	870	65	329	−309	0.0	12 27 15.77	8 22 14.0	
9991......	19.41:	1.27:	1040[a]	65	213	175	−1.4	12 27 26.38	8 14 35.4	34
9992......	19.99:	1.47:	641[a]	65	34	−27	−0.9	12 27 15.80	8 17 16.7	135

NOTE.—Successive columns give the ID, T_1 magnitude, $C - T_1$ color, heliocentric velocity, galactocentric radius, projected radius along the major axis, [Fe/H], right ascension, declination, and the identification in Table 3 of Mould et al. 1990. Units of right ascension are hours, minutes, and seconds, and units of declination are degrees, arcminutes, and arcseconds.

[a] Velocity from Mould et al. 1990.

cluster system. In particular, it reinforces the claim that the metal-rich and metal-poor populations are distinct (e.g., Zepf & Ashman 1993; Geisler et al. 1996). We investigate further the possible origins of these differences below.

3.1.1. *Rotation Velocity*

One of the key observations for testing galaxy formation models is the amount of systematic rotation in globular cluster subsystems. Since mergers are believed to be effective in transporting angular momentum outward, this provides a mechanism by which the resulting cluster population can form a dynamical system primarily supported by anisotropy rather than rotation. This natural route to hot, slowly rotating dynamical systems (at least near the center) does not arise in a (modified) monolithic-collapse picture in which dissipation is included to account for the concentrated distribution of metal-rich clusters compared with metal-poor clusters. Figure 5 shows the velocities of the globular clusters in Table 3 plotted against their radial distance projected along the major axis of NGC 4472. Formally, the least-squares fits to the metal-poor and metal-rich subpopulations are 0.57 ± 0.39 km s^{-1} arcsec^{-1} (Spearman rank correlation coefficient is 0.26) and 0.10 ± 0.31 km s^{-1} arcsec^{-1} (correlation coefficient is -0.07). However, this method assumes that the line of nodes of the cluster system is the same as that of the galaxy, which may not be the case if the system has undergone a major merger.

To constrain the rotation amplitude of the whole cluster system more generally, we have fitted a function of the form

$$V(r) = V_{\rm rot} \sin(\theta - \theta_0) + V_0 \quad (1)$$

to the radial velocity and position angle data using a nonlinear least-squares algorithm. The resulting amplitude of rotation $V_{\rm rot}$ is 85 ± 35 km s^{-1} at position angle $\theta_0 = 125° \pm 30°$, in the same sense as the rotation of the stellar component (northeast approaching, southeast receding). This is consistent with, but somewhat smaller than, the value of 113 km s^{-1} found by Mould et al. (1990) using a smaller sample. To check the reality of this result, we repeated the fit after randomizing the position angles of the clusters; in 50 trials, 12% of the fits had a rotation amplitude greater than or equal to 85 km s^{-1}, yielding a confidence level of 88% that the detected rotation is real. Since the significance of this result is not very large, we have attempted to put an upper bound on the rotation of the whole cluster system using Monte Carlo simulations. By generating artificial samples with the same position angle distribution as the data, but with velocities selected from a fixed velocity amplitude chosen to lie in the range from 50 to 250 km s^{-1} and a fixed dispersion of 258 km s^{-1}, we can put an upper limit on $V_{\rm rot}$ of 150 km s^{-1} at the 95% confidence level. As noted by Mould et al. (1990), one of their clusters (No. 19) has a significantly larger radial velocity than do any of the other clusters and should probably be excluded from the fit; Table 4 shows the corresponding values excluding this cluster.

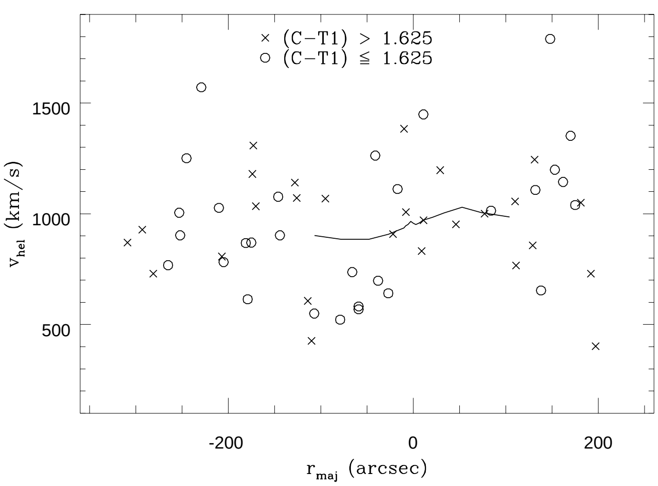

FIG. 5.—Plot of the velocities of globular clusters against their distance projected along the major axis of NGC 4472. The solid line shows the rotation of the stellar component of the galaxy from Fisher et al. (1995), normalized to the systemic velocity of the galaxy from Sandage & Tamman (1981).

Figure 6 shows the results obtained when these fits are made to the metal-rich and metal-poor subsamples separately. Although the sample size is small, there is evidence that the metal-poor (blue) clusters rotate faster than the metal-rich (red) clusters. This is opposite to what is expected in a conventional collapse picture, where the natural outcome is an old, slowly rotating, metal-poor halo population of clusters surrounding a younger, more concentrated, population of metal-rich clusters that has spun up because of conservation of angular momentum (cf. the situation in our own Galaxy). Mergers, however, provide a natural mechanism for transfer of angular momentum from the metal-rich to the metal-poor clusters. There is also a hint in Table 4 that the rotation axis for the metal-rich clusters may not be the same as that of the stellar component (P.A. = 162°) and the blue clusters. This is also what might be expected in the merger picture, although given the small number of clusters, the statistical significance is weak.

3.2. *Velocity Dispersion*

Figure 7 illustrates the velocity dispersion profile of the globular cluster system of NGC 4472. Flat rotation curves with the amplitudes given in Table 4 have been subtracted from the blue and red populations independently. The circles show the robust estimators of velocity dispersion and errors using the ROSTAT code (Bird & Beers 1993) with all the data included; the squares show the effects of removing cluster 19 from the sample (note that although cluster 19 is only in the final radial bin, removing it from the sample affects all the points, since the rotation velocity correction is

TABLE 4

RESULTS FROM NONLINEAR FITS OF EQUATION (1) TO GLOBULAR CLUSTER SAMPLES TAKEN FROM TABLE 3

Sample (1)	$V_{\rm rot}$ (km s^{-1}) (2)	θ_0 (deg) (3)	V_0 (km s^{-1}) (4)	Confidence (%) (5)	$V_{\rm rot}^{\rm max}$ (95%) (km s^{-1}) (6)
All clusters ($N = 57$)	85 (71)	125	970	88	150
Excluding No. 19 ($N = 56$)......	67 (45)	112	956	78	150
Blue clusters ($N = 30$)	159 (142)	131	1038	99	225
Excluding No. 19 ($N = 29$)......	117 (92)	122	1010	96	175
Red clusters ($N = 27$)	50 (7)	83	917	28	100

NOTE.—Column (4) contains the confidence level in $V_{\rm rot}$ obtained by randomizing the position angles of the observed clusters. Column (5) contains the 2 σ (95% confidence) upper limits to the rotation velocity obtained from Monte Carlo simulations. The values of $V_{\rm rot}$ in parentheses are those obtained when the position angle of the line of nodes is held fixed at P.A. = 162°.

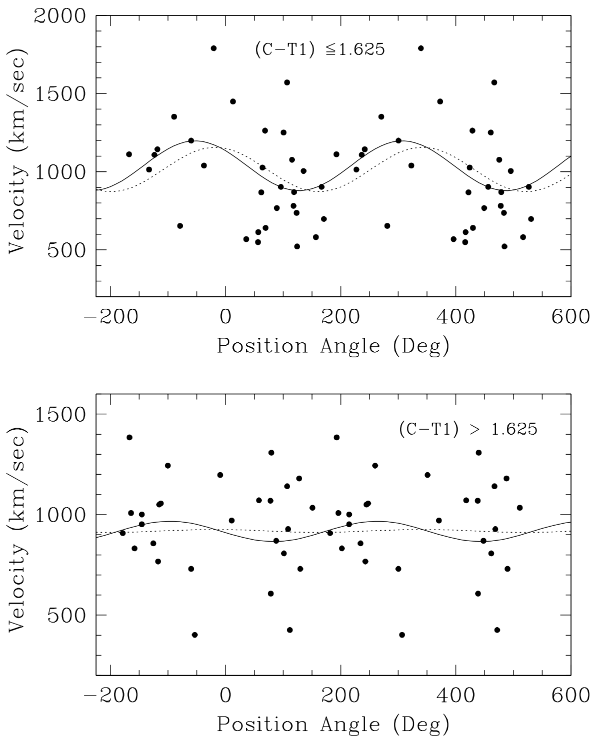

FIG. 6.—Plot of the velocities of globular clusters against their position angle (measured north through east). The major axis of NGC 4472 is at P.A. = 162°, and two complete phases are shown for clarity. The top panel shows the results for the metal-poor ($C - T_1 \leq 1.625$) clusters; the bottom panel shows the metal-rich ($C - T_1 > 1.625$) clusters. Nonlinear least-squares fits to eq. (1) are shown by the solid lines; the dashed lines show the best fit if the position angle is constrained to be 162°.

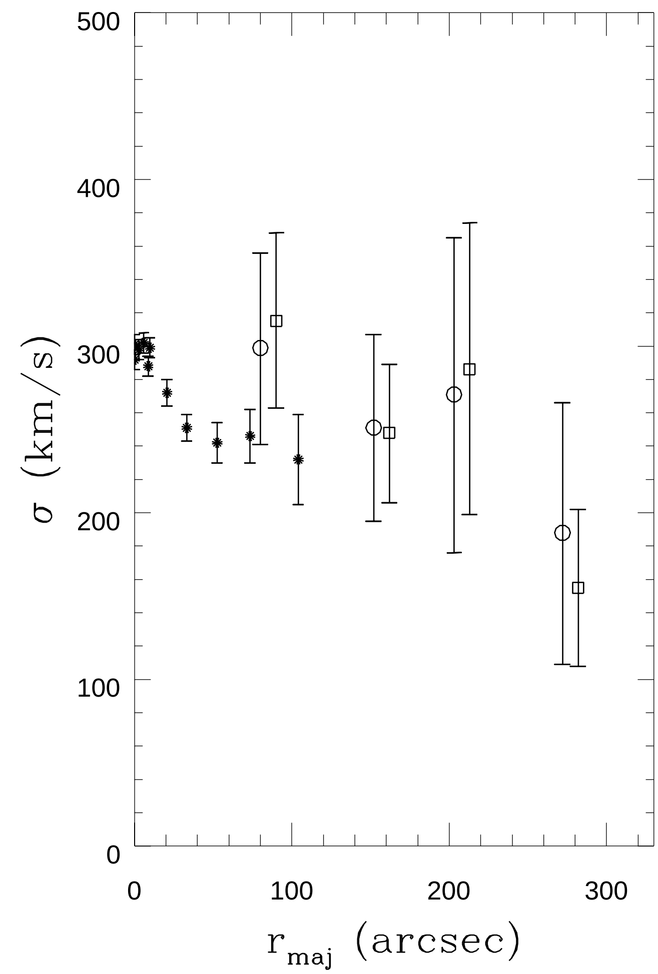

FIG. 7.—Plot of the velocity dispersion of the globular clusters in NGC 4472 against the projected distance along the major axis. Circles represent the full sample, while squares are excluding cluster 19. The velocity dispersion of the stellar light is shown by the asterisks. The importance of globular cluster samples in probing the outer halos of elliptical galaxies is clearly shown in this plot.

also different, cf. Table 4). Also plotted are the stellar velocity dispersion data for the integrated light of the galaxy from Fisher, Franx, & Illingworth (1995). The clusters appear to form a hotter dynamical population than do the halo stars, but unlike the case of M87 (Cohen & Ryzhov 1997), the dispersion profile does not increase with radius. Because the clusters and stars are known to have different structural profiles (Lee et al. 1998), they may still, of course, be in dynamical equilibrium with a single halo mass distribution.

3.3. *Mass-to-Light Ratio*

The halo mass distribution of elliptical galaxies is poorly known because of the lack of easily observed tracers such as cold H I gas. Globular clusters provide a potentially very important probe of the outer regions of elliptical galaxies (see, e.g., Cohen & Ryzhov 1997) to complement the use of planetary nebulae (Ciardullo, Jacoby, & Dejonghe 1993) and X-ray gas (Nulsen & Böhringer 1995). Figure 8 shows the integrated mass distribution for NGC 4472. The squares are X-ray estimates from Irwin & Sarazin (1996). The circle shows the projected mass estimator of Heisler et al. (1985) applied to our globular cluster sample assuming isotropic orbits and an extended mass distribution. The assumption of a point-mass distribution would decrease the projected mass estimator by a factor of ~2, but this assumption is clearly inconsistent with the extended mass profile implied by the X-ray data. More likely, the slightly higher mass estimate from the globular cluster data reflects a tangential anisotropy in the orbits, and there is some evidence to support this in our rotation analysis of the clusters. Correct-

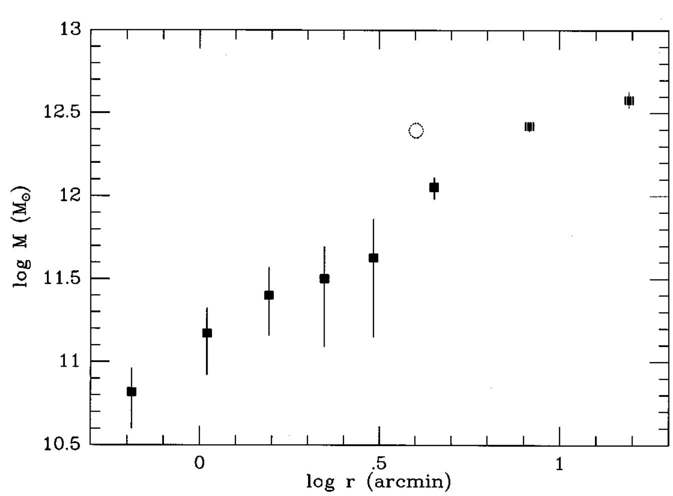

FIG. 8.—Integrated mass distribution for NGC 4472. The squares (with error bars) are the X-ray estimates from Irwin & Sarazin (1986). The circle shows the projected mass estimator applied to the globular cluster population. All mass estimates have been scaled to a Virgo Cluster distance of 16 Mpc.

ing the velocities for our best-fit rotation solution decreases the projected mass estimator by $\sim 20\%$. More important, any tendency for the cluster populations to have *radially* anisotropic orbits, as might be expected in a monolithic-collapse scenario, would increase the projected mass estimator even further above that derived from the X-ray gas.

We have calculated the M/L_B ratio using a standard B-band growth curve from the RC3 (de Vaucouleurs et al. 1991), assuming a distance to Virgo of 16 Mpc. At a projected distance of $\sim 2.5R_e$ (4′), the projected mass estimator yields $M \approx 2.5 \times 10^{12}\ M_{\odot}$, which implies that $M/L_B \approx 50$ $(M/L)_{\odot}$. This may be compared with a value of $M/L_B \approx 7$ $(M/L)_{\odot}$ derived by Saglia et al. (1993) from the stellar kinematics of the integrated light. Clearly, these kinematic studies indicate that the M/L ratio increases rapidly with radius and support the conclusion from X-ray measurements that NGC 4472 has an extended dark matter distribution similar to (although possibly not as extreme as) that seen in M87.

4. CONCLUSIONS

We have made a detailed spectroscopic study of the globular cluster system of NGC 4472 and have more than doubled the number of confirmed clusters, to 57. While this remains a statistically small sample, the data show several interesting properties when combined with the accurate color/metallicity data from Geisler et al. (1996). When the complete sample is divided into a metal-rich (47%) and a metal-poor (53%) subset on the basis of their bimodal color histogram, the metal-poor subset appears to have a broader distribution of velocities. We have investigated this further and conclude that the most likely cause is a higher mean level of rotation in the metal-poor cluster system, which is consistent with that of the underlying stellar halo in amplitude and position angle (but with a much higher specific angular momentum). The metal-rich clusters, on the other hand, show only weak evidence for any rotation, about an axis that is tilted $\sim 50°$ from that of the other components. These results are qualitatively in agreement with the predictions of a model in which the metal-rich clusters are formed during the merger of two massive gas-rich galaxies, each with its own old metal-poor cluster population. The cluster system of NGC 4472 forms a dynamically hotter population than the stellar halo, but is consistent with being in dynamical equilibrium with the halo potential defined by the hot X-ray–emitting plasma, and supports the presence of a dark $\sim 10^{12}\ M_{\odot}$ halo in this giant elliptical galaxy.

We thank Ken Freeman for useful discussions, Karl Glazebrook for his updates to the UNIX version of the LEXT data reduction package, and Jeremy Mould for providing finding charts to identify previously observed clusters. S. E. Z. acknowledges receipt of a Hubble Fellowship. D. A. H. would like to acknowledge support through an operating grant awarded by the Natural Sciences and Engineering Research Council of Canada. This work was undertaken with the support of NATO Collaborative Research Grant 941223 and is supported in part by NASA grant GO-06699.01-95A (to D. G.) from the Space Telescope Science Institute, which is operated by the Association of Universities for Research in Astronomy, Inc., under NASA contract NAS 5-26555.

REFERENCES

Allington-Smith, J. R., et al. 1994, PASP, 106, 983
Arimoto, N., & Yoshii, Y. 1987, A&A, 173, 23
Ashman, K. M., Bird, C. M., & Zepf, S. E. 1994, AJ, 108, 2348
Ashman, K. M., & Zepf, S. E. 1992, ApJ, 384, 50
———. 1997, Globular Cluster Systems (Cambridge: Cambridge Univ. Press)
Bird, C. M., & Beers, T. C. 1993, AJ, 105, 1596
Bridges, T. J., Ashman, K. M., Zepf, S. E., Carter, D., Hanes, D. A., Sharples, R. M., & Kavelaars, J. J. 1997, MNRAS, 284, 376
Ciardullo, R., Jacoby, G. H., & Dejonghe, H. B. 1993, ApJ, 414, 454
Cohen, J. G., & Ryzhov, A. 1997, ApJ, 486, 230
Cole, S., Aragon-Salamanca, A., Frenk, C. S., Navarro, J., & Zepf, S. E. 1994, MNRAS, 271, 781
de Vaucouleurs, G., de Vaucouleurs, A., Corwin, H. G. Jr., Buta, R., Paturel, G., & Fouqué, P. 1991, Third Reference Catalogue of Bright Galaxies (New York: Springer)
Fisher, D., Franx, M., & Illingworth, G. 1995, ApJ, 448, 119
Forbes, D. A., Brodie, J. P., & Grillmair, C. J. 1997, AJ, 113, 1652
Geisler, D. 1996, AJ, 111, 480
Geisler, D., Lee, M. G., & Kim, E. 1996, AJ, 111, 1529
Heisler, J., Tremaine, S., & Bahcall, J. N. 1985, ApJ, 298, 8
Hernquist, L. 1993, ApJ, 409, 548
Hesser, J. E., Shawl, S. J., & Meyer, J. E. 1986, PASP, 98, 403
Heyl, J. S., Hernquist, L., & Spergel, D. N. 1996, ApJ, 463, 69
Irwin, J. A., & Sarazin, C. L. 1996, ApJ, 471, 683
Kauffmann, G. 1996, MNRAS, 281, 487
Lee, M. G., Kim, E., & Geisler, D. 1998, AJ, in press
Mould, J. R., Oke, J. B., de Zeeuw, P. T., & Nemec, J. M. 1990, AJ, 99, 1823
Nulsen, P. E. J., & Böhringer, H. 1995, MNRAS, 274, 1093
Saglia, R. P., et al. 1993, ApJ, 403, 567
Sandage, A., & Tammann, G. A. 1981, A Revised Shapley-Ames Catalog of Bright Galaxies (Washington: Carnegie Inst. Washington)
Whitmore, B. C., Sparks, W. B., Lucas, R. A., Machetto, F. D., & Biretta, J. A. 1995, ApJ, 454, L73
Zepf, S. E., & Ashman, K. M. 1993, MNRAS, 264, 611